Mechanobiochemical finite element model to analyze impact-loading-induced cell damage, subsequent proteoglycan loss, and anti-oxidative treatment effects in articular cartilage

Citation: Kosonen, J.P., Eskelinen, A.S.A., Orozco, G.A. et al. Mechanobiochemical finite element model to analyze impact-loading-induced cell damage, subsequent proteoglycan loss, and anti-oxidative treatment effects in articular cartilage. Biomech Model Mechanobiol 24, 1191–1206 (2025).

Published Version: https://doi.org/10.1007/s10237-025-01961-8

Publisher: Springer Berlin Heidelberg

Permanent Link: https://hdl.handle.net/1721.1/163605

Version: Final published version: final published article, as it appeared in a journal, conference proceedings, or other formally published context

Biomechanics and Modeling in Mechanobiology (2025) 24:1191–1206
https://doi.org/10.1007/s10237-025-01961-8

ORIGINAL PAPER

Mechanobiochemical finite element model to analyze impact-loading-induced cell damage, subsequent proteoglycan loss, and anti-oxidative treatment effects in articular cartilage

Joonas P. Kosonen[1] · Atte S. A. Eskelinen[1] · Gustavo A. Orozco[1] · Mitchell C. Coleman[2] · Jessica E. Goetz[2] · Donald D. Anderson[2] · Alan J. Grodzinsky[3] · Petri Tanska[1] · Rami K. Korhonen[1]

Received: 26 September 2024 / Accepted: 5 April 2025 / Published online: 10 May 2025

Abstract

Joint trauma often leads to articular cartilage degeneration and post-traumatic osteoarthritis (PTOA). Pivotal determinants include trauma-induced excessive tissue strains that damage cartilage cells. As a downstream effect, these damaged cells can trigger cartilage degeneration via oxidative stress, cell death, and proteolytic tissue degeneration. N-acetylcysteine (NAC) has emerged as an antioxidant capable of inhibiting oxidative stress, cell death, and cartilage degeneration post-impact. However, the temporal effects of NAC are not fully understood and remain difficult to assess solely by physical experiments. Thus, we developed a computational finite element analysis framework to simulate a drop-tower impact of cartilage in Abaqus, and subsequent oxidative stress-related cell damage, and NAC treatment upon cartilage proteoglycan content in Comsol Multiphysics, based on prior ex vivo experiments. Model results provide evidence that immediate NAC treatment can reduce proteoglycan loss by mitigating oxidative stress, cell death (improved proteoglycan biosynthesis), and enzymatic proteoglycan depletion. Our simulations also indicate that delayed NAC treatment may not inhibit cartilage proteoglycan loss despite reduced cell death after impact. These results enhance understanding of the temporal effects of impact-related cell damage and treatment that are critical for the development of effective treatments for PTOA. In the future, our modeling framework could increase understanding of time-dependent mechanisms of oxidative stress and downstream effects in injured cartilage and aid in developing better treatments to mitigate PTOA progression.

Keywords Post-traumatic osteoarthritis · Cell death · Oxidative stress · Proteoglycan · Anti-oxidative treatment · Finite element model

✉ Joonas P. Kosonen
joonas.kosonen@uef.fi

Atte S. A. Eskelinen
atte.eskelinen@uef.fi

Gustavo A. Orozco
gustavo.orozco@uef.fi

Mitchell C. Coleman
mitchell-coleman@uiowa.edu

Jessica E. Goetz
jessica-goetz@uiowa.edu

Donald D. Anderson
don-anderson@uiowa.edu

Alan J. Grodzinsky
alg@mit.edu

Petri Tanska
petri.tanska@uef.fi

Rami K. Korhonen
rami.korhonen@uef.fi

[1] Department of Technical Physics, University of Eastern Finland, Kuopio, Finland

[2] Departments of Orthopedics and Rehabilitation and Biomedical Engineering, University of Iowa, Iowa, USA

[3] Departments of Biological Engineering, Electrical Engineering and Computer Science, and Mechanical Engineering, Massachusetts Institute of Technology, Cambridge, USA

1 Introduction

Disturbances in articular joint homeostasis after traumatic injuries, such as intra-articular fractures and anterior cruciate ligament rupture, can ultimately lead to post-traumatic osteoarthritis (PTOA) characterized by pain, stiffness, and cartilage degeneration (Anderson et al. 2011; Wang et al. 2020; Mahmoudian et al. 2021). Although the mechanisms of PTOA onset are not fully understood, several studies have shown that chondrocytes (cartilage cells) play a key role in cartilage health after impact (Anderson et al. 2011; Bartell et al. 2015; Lieberthal et al. 2015; Bonnevie et al. 2018). The cell-driven degeneration of the tissue has been suggested to be triggered by inflammation (Lieberthal et al. 2015) and trauma-related alterations in cell mechanotransduction due to excessive tissue strains or strain rates (Bartell et al. 2015; Bonnevie et al. 2018; Argote et al. 2019). Excessive mechanical strains can deform and damage the cells in cartilage, with a downstream effect of promoting excessive production of reactive oxygen species (ROS) that cause oxidative stress (Brouillette et al. 2014; Bonnevie et al. 2018). Damaged cells experiencing oxidative stress can undergo cell death, whether through necrosis or apoptosis, which decreases biosynthesis of proteoglycan molecules in the extracellular matrix (ECM) (Torzilli et al. 1999; Lepetsos and Papavassiliou 2016). In addition, excessive amounts of ROS in damaged cells can act as secondary messengers that upregulate the release of proteolytic enzymes, such as aggrecanase and collagenase enzymes, that further increase the loss of the ECM components (Hodgkinson et al. 2022; Riegger et al. 2023).

Orally or intra-articularly delivered antioxidants can reduce the amount of ROS directly by scavenging ROS and indirectly by fortifying the natural antioxidative system within chondrocytes (Aldini et al. 2018; Tudorachi et al. 2021; Riegger et al. 2023). Several antioxidants have been studied (Setti et al. 2021; Tudorachi et al. 2021), and N-acetylcysteine (NAC) has emerged as one of the most potent antioxidants in inhibiting cell death and reducing ECM degeneration after *ex vivo* impact (Martin et al. 2009; Riegger et al. 2016, 2018, 2019; Coleman et al. 2018). In addition, intra-articularly delivered NAC has shown promising results in animal models *in vivo* (porcine, rabbit, rat) with reduced oxidative stress, cell death, and proteoglycan loss 2–6 months after joint injury (Nakagawa et al. 2010; Coleman et al. 2018; Riegger et al. 2019). Compared to hyaluronic acid treatment, NAC also reduced inflammatory and cartilage degeneration markers in a pilot study of intra-articular treatment of patients with moderate OA ($n = 20$, Kellgren-Lawrence grade 2–3) (Ozcamdalli et al. 2017). Despite the positive effects of intra-articular NAC in the previous experiments, long-term oral NAC treatment has been shown to increase the risk of OA (Yeh et al. 2020). Hence, finding an optimal delivery method, dosage, and timing sufficient to inhibit post-impact cell damage and later cartilage degeneration in vivo is critically important and remains difficult due to the rapid clearance of the small NAC molecules (163 Da) from the synovial fluid (Siefen et al. 2022).

Computational models have proved useful for estimating cartilage response to injurious loading, progression of cartilage degeneration, and treatment effects. Biomechanical finite element models with stress/strain-based degeneration algorithms have been used for simulating tissue degeneration under physiologically relevant loading conditions (Hosseini et al. 2014; Orozco et al. 2018; Eskelinen et al. 2019; Elahi et al. 2023). Recently, these biomechanical degeneration models have been coupled with biological mechanisms, such as time-dependent diffusion of pro-inflammatory cytokines (Kar et al. 2016a; Eskelinen et al. 2020), biomechanically triggered ROS overproduction (Kosonen et al. 2023), cell death (Kapitanov et al. 2016), and enzymatic degeneration of proteoglycans (Kar et al. 2016a). Building on these mechanobiological degeneration models, recent work has simulated the effects of anti-inflammatory treatments on time-dependent cartilage degeneration (Kar et al. 2016b; Rahman et al. 2023). Yet, there are no models combining injurious loading, oxidative stress-induced cell damage, and damaged cell-driven degeneration of cartilage with computational simulation of antioxidant treatment aiming to prevent cellular oxidative injury following a high-energy impact. Such models could be used to explore why an intra-articular anti-oxidative injection may or may not work in any given clinically relevant scenario (type of injury, treatment timing, dosage, etc.).

In this study, we developed a new computational modeling framework to simulate a high-energy impact, impact-induced oxidative cell damage, acute cell death and adaptation of proteoglycan content. This framework was then used to simulate the effects of short-term NAC treatment in mature bovine cartilage, with an aim to understand which mechanobiologically relevant modeling parameters can explain the cell viability and proteoglycan content measured quantitatively in prior experiments (Martin et al. 2009). We hypothesized that i) higher proteoglycan content in immediately NAC treated vs. untreated samples after impact could be partly explained by inhibited strain-induced local cell oxidative damage, proteolytic degeneration of proteoglycans, and cell death, and that ii) although impact-induced oxidation driven cell death could be inhibited with NAC treatment delivered at a later time point after mechanical impact, delayed treatment is insufficient to fully protect matrix proteoglycan content due to substantial release of proteolytic enzymes before the treatment. Due to a lack of accurate and repeatable measures of cell-level parameters such as cell death rate and chondrocyte protection rate by NAC, we

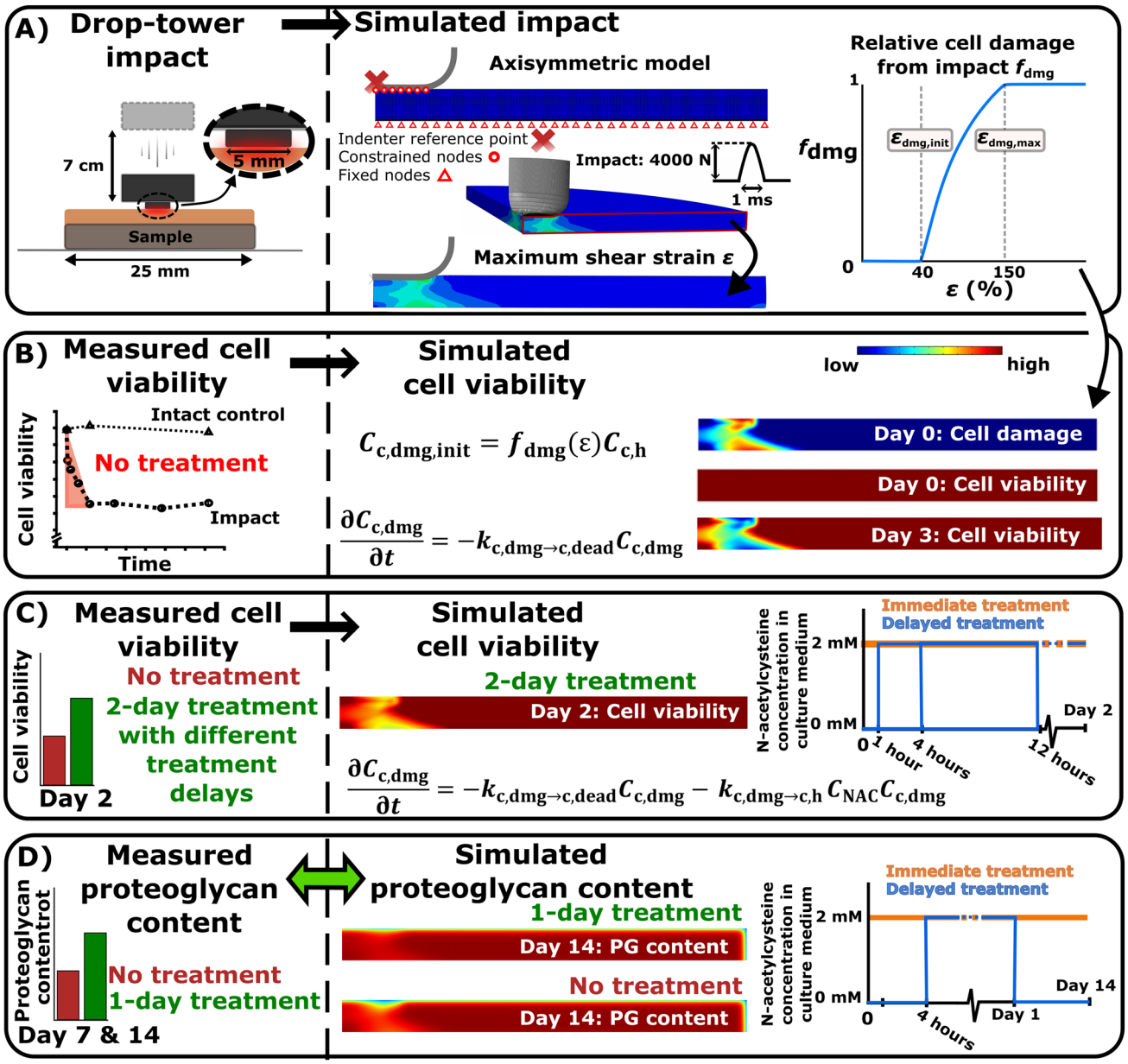

Fig. 1 Workflow. **A** The biomechanical response of cartilage to drop-tower impact was first simulated based on prior experiments. Maximum shear strains were computed at the time of peak impact force (4000N) to identify cell damage (i.e., cells experiencing oxidative stress). **B** Time-dependent loss of cell viability from impact was next simulated for comparison with experimental findings. **C** Then, N-acetylcysteine (NAC)-induced cell recovery after 0, 1, 4, and 12-h post-impact treatment delay was simulated, and viability was matched with experiments. **D** Finally, proteoglycan degeneration driven by the damaged cells and the mitigating effect of NAC treatment was simulated

investigated the effect of the most important parameters on cell death and proteoglycan content via sensitivity analysis. This approach marks an important step toward understanding and numerically estimating the underlying mechano-biological effects of antioxidant treatment at cell and tissue levels in cartilage after severe impact injury. Ultimately, our modeling framework could help in designing more efficient treatments to mitigate PTOA.

2 Methods

2.1 Previous experiments as a basis of the computational framework

Our computational modeling framework leverages prior *ex vivo* drop-tower impact experiments of mature bovine osteochondral plugs (25 mm wide) conducted by Martin et al. (Martin et al. 2009) (Fig. 1A). The following experimental data were compared against the results from our computational model: **1)** cell viability in untreated samples 200 µm from the impacted surface (confocal microscopy) 1-, 3-, 6-, 12-, 24-, and 48-h after impact (Fig. 1A and B), **2)** cell viability in samples treated with NAC (2 mM) at day 2 with 0-, 1-, 4-, and 12-h treatment delay (Fig. 1C), and **3)** relative proteoglycan content at days 7 and 14 post-impact in samples with and without immediate 1-day NAC treatment (Fig. 1D). In the experiments, the relative proteoglycan content was quantified with dimethyl methylene blue assay of 4 mm wide impacted vs. intact regions dissected from original samples (Martin et al. 2009).

2.2 Finite element model for simulating impact loading and shear strain-triggered cell damage

An axisymmetric finite element model of the cartilage (width of 12.5 mm, height of 1 mm) and a bevelled flat-ended indenter (5 mm diameter with 1 mm circle radius for the rounded edge) was constructed to simulate the impact. Cartilage was modeled as a continuum-level fibril-reinforced poroviscoelastic material with chemical expansion and Donnan osmotic swelling, which separately considers the effect of solid non-fibrillar (hyperelastic Neo-Hookean material) and fibrillar matrix, as well as fluid flow within the tissue (Darcy's law with deformation-dependent permeability), for the mechanical response of cartilage (Wilson et al. 2004, 2005c, b). In the material model, the Cauchy stress tensor for the hyperelastic Neo-Hookean material $\boldsymbol{\sigma}_{\mathrm{nf}}$ was modeled as

$$\boldsymbol{\sigma}_{\mathrm{nf}} = \frac{E_{\mathrm{nf}}}{3\left(1-2\nu_{\mathrm{nf}}\right)}\frac{\ln(J)}{J}\mathbf{I} + \frac{E_{\mathrm{nf}}}{2\left(1+\nu_{\mathrm{nf}}\right)}\frac{1}{J}\left(\mathbf{F}\cdot\mathbf{F}^{\mathrm{T}} - J^{\frac{2}{3}}\mathbf{I}\right), \tag{1}$$

where E_{nf} is the Young's modulus of the non-fibrillar matrix, ν_{nf} is the Poisson's ratio of the non-fibrillar matrix, $\mathbf{F}$ is the deformation gradient tensor, $\mathbf{I}$ is the unit tensor and $J = \det(\mathbf{F})$ is the volumetric deformation.

Collagen fiber network had the Benninghoff arcade-like architecture for the primary fibrils and random orientation for the secondary fibrils. The Cauchy stress tensor ${\boldsymbol{\sigma}_{\mathrm{f}}}^{k}$ was defined as:

$$\boldsymbol{\sigma}_{\mathrm{f}}^{k} = \begin{cases} \rho_{\mathrm{z}} C \sigma_{\mathrm{f}} \boldsymbol{e}_{\mathrm{f}} \otimes \boldsymbol{e}_{\mathrm{f}}, & \text{if } k = \text{primary}, \\ \rho_{\mathrm{z}} \sigma_{\mathrm{f}} \boldsymbol{e}_{\mathrm{f}} \otimes \boldsymbol{e}_{\mathrm{f}}, & \text{if } k = \text{secondary}, \end{cases} \tag{2}$$

where ρ_{z} is the collagen density fraction, C is the ratio between primary and secondary fibrils, $\boldsymbol{e}_{\mathrm{f}}$ is the unit vector for fibril orientation in the current configuration (Wilson et al. 2005c), $\otimes$ is the outer product operation and σ_{f} is stress of a collagen fibril (scalar). To consider viscoelastic behavior of the collagen fibrils, the fibril stress was determined as (Wilson et al. 2004, 2005b, c)

$$\sigma_{\mathrm{f}} = \begin{cases} -\frac{\eta}{2\sqrt{E_{\epsilon}\left(\sigma_{\mathrm{f}}-E_0\varepsilon_{\mathrm{f}}\right)}}\dot{\sigma}_{\mathrm{f}} + E_0\varepsilon_{\mathrm{f}} + \left(\eta + \frac{\eta E_0}{2\sqrt{E_{\epsilon}\left(\sigma_{\mathrm{f}}-E_0\varepsilon_{\mathrm{f}}\right)}}\right)\dot{\varepsilon}_{\mathrm{f}}, & \varepsilon_{\mathrm{f}} \geq 0, \\ 0, & \varepsilon_{\mathrm{f}} < 0, \end{cases} \tag{3}$$

where $\dot{\sigma}_{\mathrm{f}}$ and $\dot{\varepsilon}_{\mathrm{f}}$ are fibril stress and strain rates, η is the damping coefficient, E_0 is the initial fibril network modulus, and E_{ϵ} is the strain-dependent fibril network modulus.

Darcy's law was used to describe the fluid flow in the porous non-fibrillar matrix as

$$\overline{q} = k\nabla p, \tag{4}$$

where $\overline{q}$ is the flow flux, p is the fluid pressure, and k is the deformation-dependent permeability which was modeled as

$$k = k_0\left(\frac{1+e}{1+e_0}\right)^{M} = k_0 J^{M}, \tag{5}$$

where k_0 is the initial permeability, M is the strain-dependent permeability coefficient, e_0 and e are initial and current void ratios. Void ratio is defined as

$$e = \frac{n_{\mathrm{fl}}}{n_{\mathrm{s}}}, \tag{6}$$

where n_{fl} is fluid fraction and $n_{\mathrm{s}} = 1 - n_{\mathrm{fl}}$ is the solid fraction.

The chemical expansion stress, describing repulsion of the negative charge groups in proteoglycans, was modeled according to previous studies as (Wilson et al. 2005c, a)

$$T_{\mathrm{c}} = a_0 c_{\mathrm{FCD}} \exp\left(-\kappa\frac{\gamma_{\mathrm{ext}}^{\pm}}{\gamma_{\mathrm{int}}^{\pm}}\sqrt{c^{-}\left(c^{-}+c_{\mathrm{FCD}}\right)}\right), \tag{7}$$

where a_0 and κ are material constants, $\gamma_{\mathrm{ext}}^{\pm}$ and $\gamma_{\mathrm{int}}^{\pm}$ are external and internal activity coefficients, and c^{-} is the mobile anion concentration in the cartilage (Huyghe et al. 2003; Wilson et al. 2005c). The depth-dependent fixed charge density c_{FCD} is described as a function of volumetric deformation as

$$c_{\mathrm{FCD}} = c_{\mathrm{FCD},0}\frac{n_{\mathrm{fl},0}}{n_{\mathrm{fl},0} - 1 + J}, \tag{8}$$

where $c_{\mathrm{FCD},0}$ is the initial depth-wise fixed charge density and $n_{\mathrm{fl},0}$ is initial fluid fraction.

Donnan osmotic swelling was modeled as (Wilson et al. 2005a)

$$\Delta\pi = \phi_{\mathrm{int}} RT\left(\sqrt{c_{\mathrm{FCD}}^2 + 4\frac{\left(\gamma_{\mathrm{ext}}^{\pm}\right)^2}{\left(\gamma_{\mathrm{int}}^{\pm}\right)^2}c_{\mathrm{ext}}^2}\right) - 2\phi_{\mathrm{ext}} RTc_{\mathrm{ext}}, \quad (9)$$

where ϕ_{ext} and ϕ_{int} are external and internal osmotic coefficients (Huyghe et al. 2003), R is the molar gas constant, T is the absolute temperature, and c_{ext} is the external salt concentration.

Finally, the total stress tensor $\boldsymbol{\sigma}_{\mathrm{tot}}$ of the cartilage tissue was determined as (Wilson et al. 2004, 2005c, b)

$$\boldsymbol{\sigma}_{\mathrm{tot}} = \boldsymbol{\sigma}_{\mathrm{nf}} + \sum_{k=1}^{totf}\boldsymbol{\sigma}_{\mathrm{f}}^{k} - T_{\mathrm{c}}\mathbf{I} - \Delta\pi\mathbf{I} - \mu_{\mathrm{f}}\mathbf{I}, \quad (10)$$

where *totf* is the sum of primary and secondary fibrils, and μ_{f} is the chemical potential of water (Wilson et al. 2005a). The depth-dependent composition and structure (i.e. fixed charge density, water content, collagen density and orientation) and material parameters of the model were estimated based on prior reports of mature bovine cartilage (see visualization of the depth-dependent composition and structure in supplementary material S1) (Wilson et al. 2004, 2005c; Julkunen et al. 2007), and they are presented in table S1 in the supplementary material S1.

As an initial simulation step, cartilage was allowed to swell until mechanical equilibrium (physiological salt concentration, i.e., 0.15 M NaCl) (Wilson et al. 2005c) followed by simulation of the cartilage-indenter impact with a sinusoidal-like force. The impact loading was assigned to an indenter reference point (Fig. 1A), and the indenter was assumed rigid. Earlier drop-tower studies have reported sinusoidal-like force-responses to impact over 0.6–2 ms (Jeffrey et al. 1995; Jeffrey and Aspden 2006; Burgin and Aspden 2007), thus we assumed total impact time $t_{\mathrm{impact}} = 1$ ms (Fig. 1A, time to peak 0.5 ms). With this impact time, we calculated the average impact force ($F_{\mathrm{impact,\,av}} = mv_{\mathrm{av}}/t_{\mathrm{impact}}$, where average impact velocity $v_{\mathrm{av}} = \sqrt{2gh}$, m is the mass of the impactor, g is the gravity constant, and h is drop height of the impactor) of the 7 J/m^2 to be $F_{\mathrm{impact,\,av}} = 2350$ N (average stress $\sigma_{\mathrm{impact,\,av}} = 120$ MPa) and corresponding peak impact force to be $F_{\mathrm{impact,\,peak}} = 4000$ N (Fig. 1A; peak impact stress $\sigma_{\mathrm{peak}} = 200$ MPa, 400 GPas^{-1} loading rate). We consider this peak impact force estimate reasonable, since they are in similar scale as earlier drop-tower impact experiments showing 50–70 MPa peak impact stresses (800–1100 N peak impact forces) with an indenter of 5.5 mm in diameter (Heiner et al. 2013). However, sensitivity analysis with 2000N (100 MPa peak impact stress, 200 GPa/s loading rate) and 6000N peak impact forces (300 MPa peak impact stress) were also conducted to analyze effect of the impact force and loading rate on maximum shear strain, pore pressure, and cell damage (See supplementary material S2).

Since high local strains trigger oxidative stress and cell death (Bonnevie et al. 2018), we calculated the maximum shear strain from the Green-Lagrangian strain tensor (see supplementary material S3) at the peak impact force (0.5 ms). The maximum shear strain distribution was used to define the fraction of damaged cells from initially healthy cells with a nonlinear cellular damage function $f_{\mathrm{dmg}}(\varepsilon)$ (Hosseini et al. 2014):

$$f_{\mathrm{dmg}}(\varepsilon) = \begin{cases} 0, & \text{when } \varepsilon < \varepsilon_{\mathrm{dmg,init}} \\ \frac{\varepsilon_{\mathrm{dmg,max}}}{\varepsilon}\frac{\varepsilon-\varepsilon_{\mathrm{dmg,init}}}{\varepsilon_{\mathrm{dmg,max}}-\varepsilon_{\mathrm{dmg,init}}}, & \text{when } \varepsilon_{\mathrm{dmg,init}} \le \varepsilon \le \varepsilon_{\mathrm{dmg,max}} \\ 1, & \text{when } \varepsilon > \varepsilon_{\mathrm{dmg,max}} \end{cases} \quad (11)$$

where ε is the maximum shear strain, $\varepsilon_{\mathrm{dmg,init}} = 40\%$ is the strain threshold describing the initiation of cell damage, and $\varepsilon_{\mathrm{dmg,max}} = 150\%$ is the maximum cell damage threshold describing the limit when all cells are damaged (Argote et al. 2019). This initial cell damage was used as an input for the cell viability and proteoglycan content simulations (see Sect. 2.3, Eq. 16).

The biomechanical model to simulate the mechanical cartilage response in the drop-tower impact experiment was constructed in Abaqus (v. 2023, Dassault Systèmes, Providence, RI, USA) with 2506 continuum pore pressure elements (type: CAX4P) and solved with transient soils consolidation analysis. Indenter-cartilage contact was modeled using tabular pressure–overclosure relationship in the axial direction and frictionless in the radial direction. The contact area during the impact was assumed constant, thus, nodes of the cartilage geometry initially in contact with the indenter were constrained in the radial direction during the simulations. The bottom surface of the cartilage tissue was fixed in axial and radial directions (osteochondral plug in Martin et al. (Martin et al. 2009); bone was not included in the model). Fluid flow and radial movement of the nodes was prevented on the symmetry axis of the plug (axisymmetric boundary condition). Fluid flow was allowed through the free boundaries. Mesh convergence was verified (see Supplementary material S4).

2.3 Modeling cell viability, proteoglycan degeneration, and NAC treatment

In our modeling framework (Fig. 2), we simulated distributions of healthy, damaged and dead cells, where initially healthy cells were turned into damaged cells due to excessive

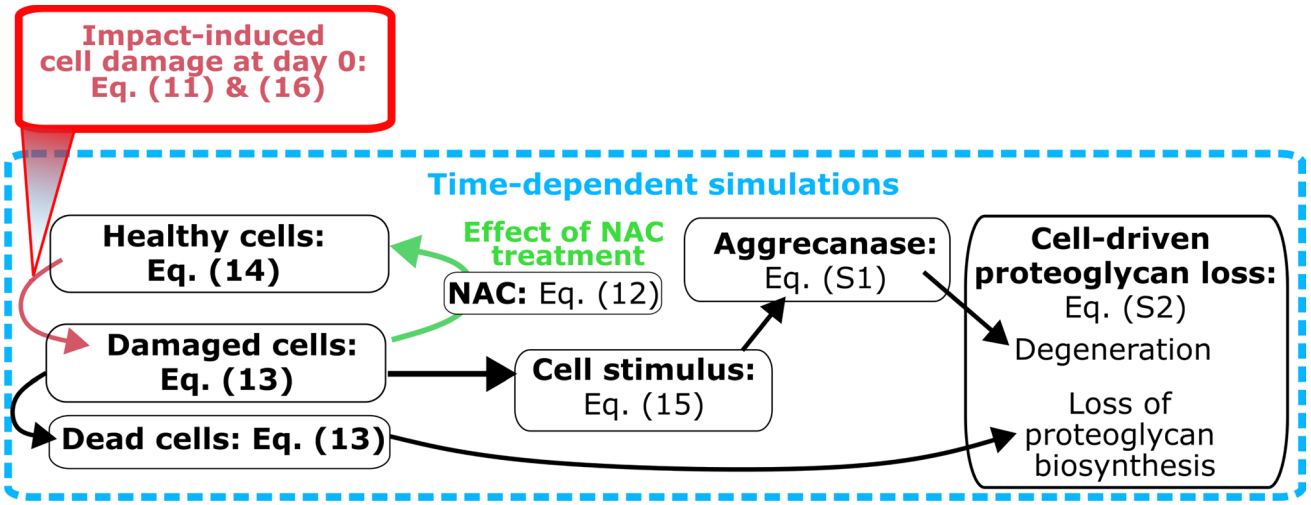

Fig. 2 Overview of the modeling framework. Visualization of the cell-driven proteoglycan degeneration and the effect of NAC treatment implemented in the model

local strains caused by the impact (Eq. 11). The damaged cell population was assumed to have less efficient antioxidative defenses, thus they were allowed to die over time due to being more susceptible to oxidative stress after the impact (Sauter et al. 2012; Coleman et al. 2016, 2017). In the model, the cells in a damaged state released proteolytic enzymes that could degenerate proteoglycans and no purely mechanically induced degeneration was considered. The total biosynthesis of proteoglycans in cartilage was decreased due to lower number of viable cells (healthy + damaged). The cell damage was mitigated by diffusion of NAC from the free tissue boundaries, inhibiting the downstream effects of cell damage and restoring the antioxidative defense system of the cells rendering them back into healthy cellular state (Coleman et al. 2018).

All cell-related processes were modeled in Comsol Multiphysics (v. 5.6, Burlington, MA, USA) with reaction–diffusion partial differential equations (Kar et al. 2016a; Kosonen et al. 2023):

$$\frac{\partial C_s}{\partial t} = D_s \nabla^2 C_s + R_{s,\text{source}} - R_{s,\text{sink}}, \tag{12}$$

where t is time, C_s is the concentration of a given constituent species within cartilage, D_s is the effective diffusion constant, $R_{s,\text{source}}$ is the source term, and $R_{s,\text{sink}}$ the sink term of species s (s = healthy, damaged or dead cell population or proteoglycan, proteolytic enzyme, or NAC concentration). Effective diffusion of proteolytic enzymes was modeled depth-dependent according to the defined proteoglycan content as in (Kar et al. 2016a). Source/sink terms for proteoglycans and proteolytic enzymes (describing degeneration of proteoglycans) were modeled according to Michaelis–Menten kinetics as in (Kar et al. 2016a) and (Kosonen et al. 2023). For NAC, we assumed isotropic diffusion as $D_{\text{NAC}} = 120 \cdot 10^{-6}$ m^{2}s^{-1} based on its molecular weight (163 Da) (Didomenico et al. 2018). Due to lack of experimental data regarding NAC half-life and chemical reaction rates in cartilage, source/sink terms for NAC were assumed zero (i.e., NAC was only diffusing into cartilage without further changes until free diffusion of NAC out of cartilage when culture media was changed).

Damaged chondrocytes were allowed to die due to oxidative stress. Unlike in previous studies (Kapitanov et al. 2016; Kosonen et al. 2023), we did not explicitly model ROS concentration in damaged cells due to high variation in reaction kinetics of different ROS molecules (Aldini et al. 2018). Instead, we implicitly modeled cellular oxidative stress through the concentration of damaged chondrocytes $C_{\text{c,dmg}}$, that could be further altered by the presence of NAC:

$$\frac{\partial C_{\text{c,dmg}}}{\partial t} = -k_{\text{c,dmg}\rightarrow\text{c,dead}} C_{\text{c, dmg}} - \frac{\partial C_{\text{c,h}}}{\partial t}, \tag{13}$$

where $k_{c,\text{dmg}\rightarrow c,\text{dead}}$ is the cell death rate for damaged cells, and $C_{\text{c,h}}$ is the concentration of healthy cells. Accordingly, the recovery of damaged chondrocytes back to healthy type was modeled as

$$\frac{\partial C_{\text{c,h}}}{\partial t} = k_{\text{c,dmg}\rightarrow\text{c,h}} C_{\text{NAC}} C_{\text{c,dmg}}, \tag{14}$$

where $k_{\text{c,dmg}\rightarrow\text{c,h}}$ is the chondrocyte protection rate due to NAC (recovery of damaged cells back to healthy cells) and C_{NAC} is the NAC concentration. Since Martin et al. (Martin et al. 2009) reported on average less than 5% change in

cell viability in unimpacted control samples after 3 days of culture, we did not assume spontaneous, basal chondrocyte death or recovery in our simulations.

Proteoglycan loss was modeled by simulating increased proteolytic activity observed earlier after impact injury (Ding et al. 2014; Riegger et al. 2018). The production of proteolytic enzymes was increased according to an exponential stimulus function S (for more details, see Supplementary material S5), which was elevated in the areas of damaged cells $C_{c,dmg}$:

$$\frac{\partial S}{\partial t} = \alpha_{aga}\left(k_{aga}C_{c,dmg} - S\right), \tag{15}$$

where $\alpha_{aga} = 0.4 \cdot 10^{-5}\ s^{-1}$ is the rate constant for stimulus and k_{aga} is a stimulus constant for proteolytic enzyme release from damaged cells. Initial cell stimulus and proteolytic enzyme concentration was set to zero, and zero flux for proteolytic enzymes was set at all boundaries. Initial proteoglycan concentration was calculated from the fixed charge density distribution used in the biomechanical impact model (for more details of the biochemical model, see supplementary material S5) (Wilson et al. 2004, 2005c; Orozco et al. 2022).

Due to a lack of data on cell distribution of the impacted samples in (Martin et al. 2009), initial healthy cell concentration was assumed homogeneous ($C_{c,h,init} = 0.5 \cdot 10^{14}\ m^{-3}$) (Jadin et al. 2005). Also, no cell proliferation was considered (*i.e.,* the sum of damaged, healthy, and dead cells was assumed constant $C_{c,dmg} + C_{c,h} + C_{c,dead} = C_{c,h,init}$). Assuming a fraction of cells would become damaged after impact (see Eq. 11) (Bonnevie et al. 2018), we set the initial cell damage as:

$$C_{c,dmg,\,init} = f_{dmg}(\varepsilon)C_{c,h} \tag{16}$$

The initial NAC concentration within the cartilage was set to zero, and the concentration on the free surfaces (top and outer surface) was set to 2 mM (Fig. 1C). To simulate the delayed administration of NAC (0, 1, 2, 3, 4 and 12 h after impact, Fig. 1C), the NAC concentration on the free surfaces was increased from 0 to 2 mM with a step function. Radial and axial fluxes through the boundaries for proteoglycan and proteolytic enzyme molecules were defined as described previously by Kar et al. (Kar et al. 2016a).

2.4 Sensitivity analysis and reference parameters

Sensitivity analyses were conducted to analyze the effect of relevant model parameters on the cell viability and proteoglycan content (Table 1). These parameters included the maximum cell damage threshold $\varepsilon_{dmg,max}$, cell death rate for damaged cells $k_{c,dmg\rightarrow c,dead}$, proteolytic enzyme stimulus constant in damaged cells k_{aga}, and chondrocyte protection rate after NAC treatment $k_{c,dmg\rightarrow c,h}$. Reference parameters were selected so that predicted average cell viability matched experimental outputs (Martin et al. 2009) (see Sect. 2.1). Ranges for sensitivity analysis were selected so that predicted average cell viability was within one standard deviation of the experimentally measured mean cell viability. Additionally, we conducted sensitivity analyses for the peak impact force and proteolytic enzyme stimulus constant in damaged cells to study their effect on the initial cell damage and proteoglycan loss (see supplementary material S2 and S6).

3 Results

3.1 By inhibiting cell damage in impacted cartilage, NAC partly reduced proteoglycan loss

With the reference parameters (Table 1 in Sect. 2.5), the mechanical impact model predicted cell damage extending through the full thickness of the tissue, whereas no cell damage was predicted in the non-impacted region (Fig. 3A). Without treatment, cell death was observed in the excessively loaded regions of cartilage, and NAC treatment immediately after impact inhibited the acute cell death.

The model predicted proteoglycan loss throughout the cartilage depth in the impacted area (Fig. 3B), and the lowest proteoglycan content was located at the superficial zone. Simulated NAC treatment was able to inhibit the

Table 1 Parameters for sensitivity analysis. Cell viability, proteoglycan degeneration, and treatment-related parameters chosen for the sensitivity analysis. Bolded values were chosen as the reference value

Parameters	Reference parameters	Range	Description	Reference
$\varepsilon_{dmg,max}$ [%]	**150%**	100%, **150%**, 200%	Maximum cell damage threshold	Martin et al. (2009); Argote et al. (2019)
$k_{c,dmg\rightarrow c,dead}$ [$10^{-5}\ s^{-1}$]	**6.9**	4.6, **6.9**, 13.9	Cell death rate for damaged cells	Martin et al. (2009)
$k_{c,dmg\rightarrow c,h}$ [$10^{-4} m^3 mol^{-1}\ s^{-1}$]	**0.53**	0.29, 0.39, **0.53**	Chondrocyte protection rate	Martin et al. (2009)

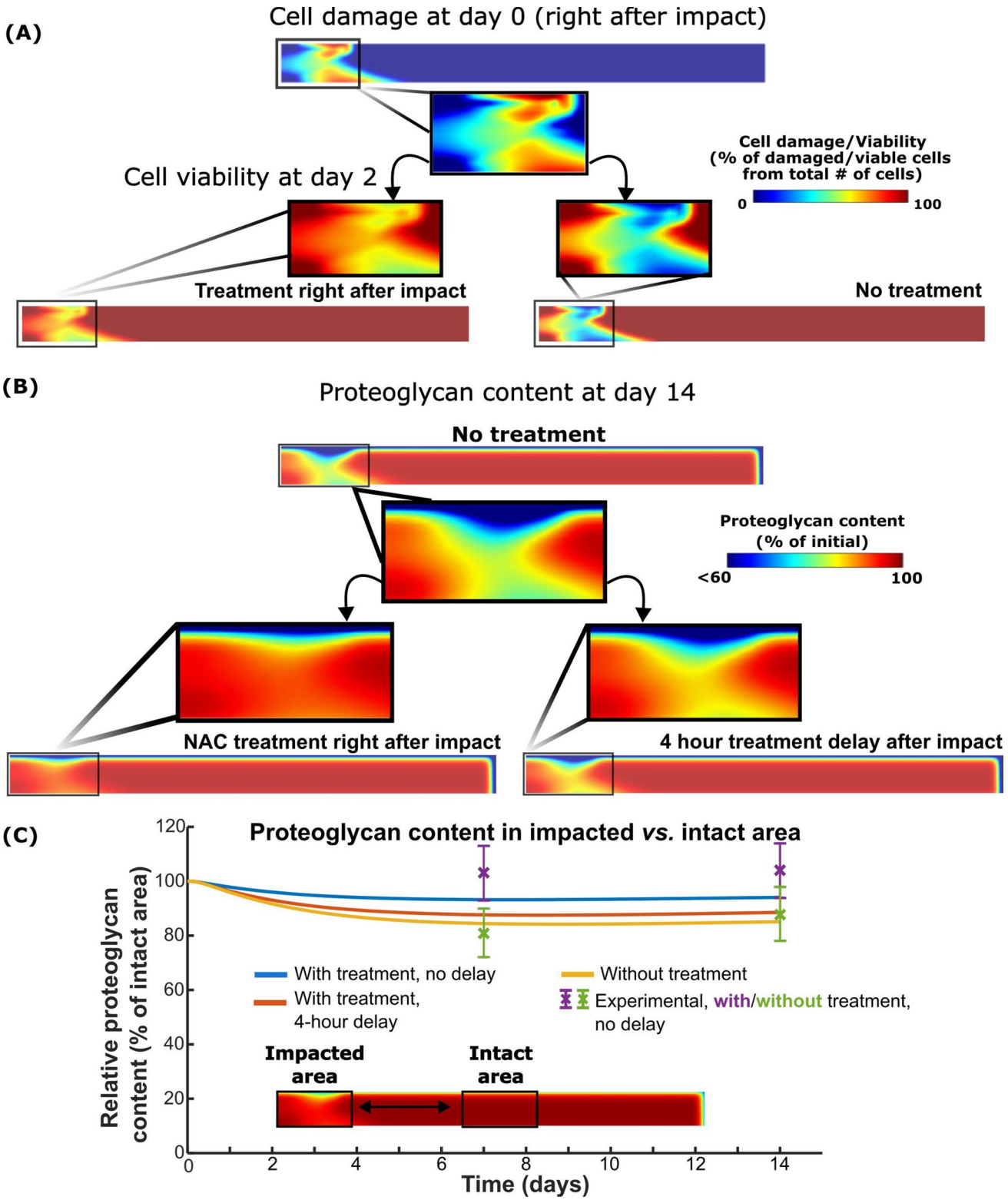

Fig. 3 NAC can reduce proteoglycan loss by inhibiting impact-induced cell damage. **A** Our simulations showed high cell damage after impact, leading to acute cell death in damaged regions. Immediate post-impact NAC treatment effectively preserved cell viability throughout cartilage depth in the damaged areas. **B** Without NAC treatment, proteoglycan content was subsequently reduced throughout the depth of the cartilage. Immediate post-impact NAC treatment inhibited proteoglycan loss by reducing cell damage, but treatment after a 4-h delay was less successful in maintaining proteoglycan content. **C** Quantitatively, our simulated results matched experiments and showed that 4-h treatment delay resulted in proteoglycan content resembling the content in untreated cartilage after impact

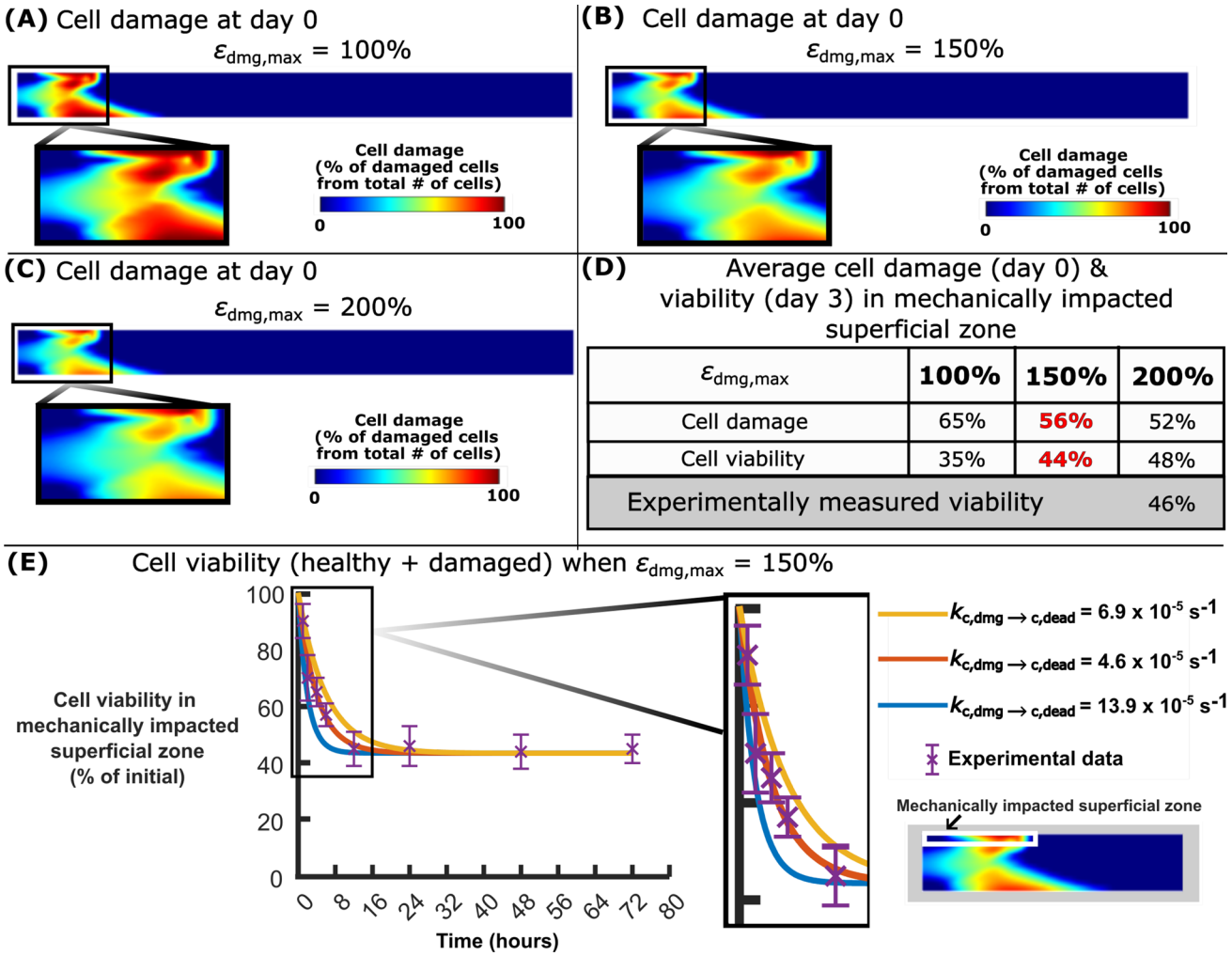

$\varepsilon_{dmg,max}$	100%	150%	200%
Cell damage	65%	**56%**	52%
Cell viability	35%	**44%**	48%
Experimentally measured viability			46%

Fig. 4 Calibration of cell damage and viability after impact. Cell damage distributions at day 0 after impact, when **A** the maximum cell damage threshold $\varepsilon_{dmg,max}$ = 100%, **B** when $\varepsilon_{dmg,max}$ = 150%, and **C** when $\varepsilon_{dmg,max}$ = 200%. Since **D** $\varepsilon_{dmg,max}$ = 150% best matched the experiments, **E** it was utilized to determine the cell death rate for damaged cells $k_{c,d \rightarrow c,dead}$ over 72 h after impact. With $k_{c,d \rightarrow c,dead}$ = 6.9×10^{-5} s^{-1}, the model replicated also the decrease in cell viability (amount of healthy cells maintained) during the first 16 h after impact. Experimental data show the mean ± standard deviation

proteoglycan content loss in the impacted area when the treatment was administered immediately after the impact loading. Four hours post-impact treatment delay resulted in proteoglycan loss in the superficial and deeper parts of the cartilage closer to that in the untreated samples. Most of the proteoglycan loss was observed within 7 days after impact, and on day 14, the predicted proteoglycan content was 5%, 11% and 14% lower in the impacted region compared to the intact region in immediately treated, 4-h treatment delay, and without treatment models (Fig. 3C).

3.2 Sensitivity analysis of cell damage and predicted cell viability after delayed treatment

Increasing the $\varepsilon_{dmg,max}$ threshold (Table 1) resulted in lower cell damage in the impacted area (Fig. 4A–C), while the opposite was observed when decreasing the threshold. That is, $\varepsilon_{dmg,max}$ = 100% resulted in 65% cell damage for the initially healthy cells in the impacted superficial zone, whereas the reference value $\varepsilon_{dmg,max}$ = 150% led to 56% and $\varepsilon_{dmg,max}$ = 200% to 52% cell damage. By selecting $\varepsilon_{dmg,max}$ = 150% (Fig. 4D), the reference model (with $k_{c,dmg \rightarrow c,dead} = 6.9 \cdot 10^{-5}$ s^{-1}, Table 1) replicated well the average cell viability (46%) observed in experiments three days after the impact loading

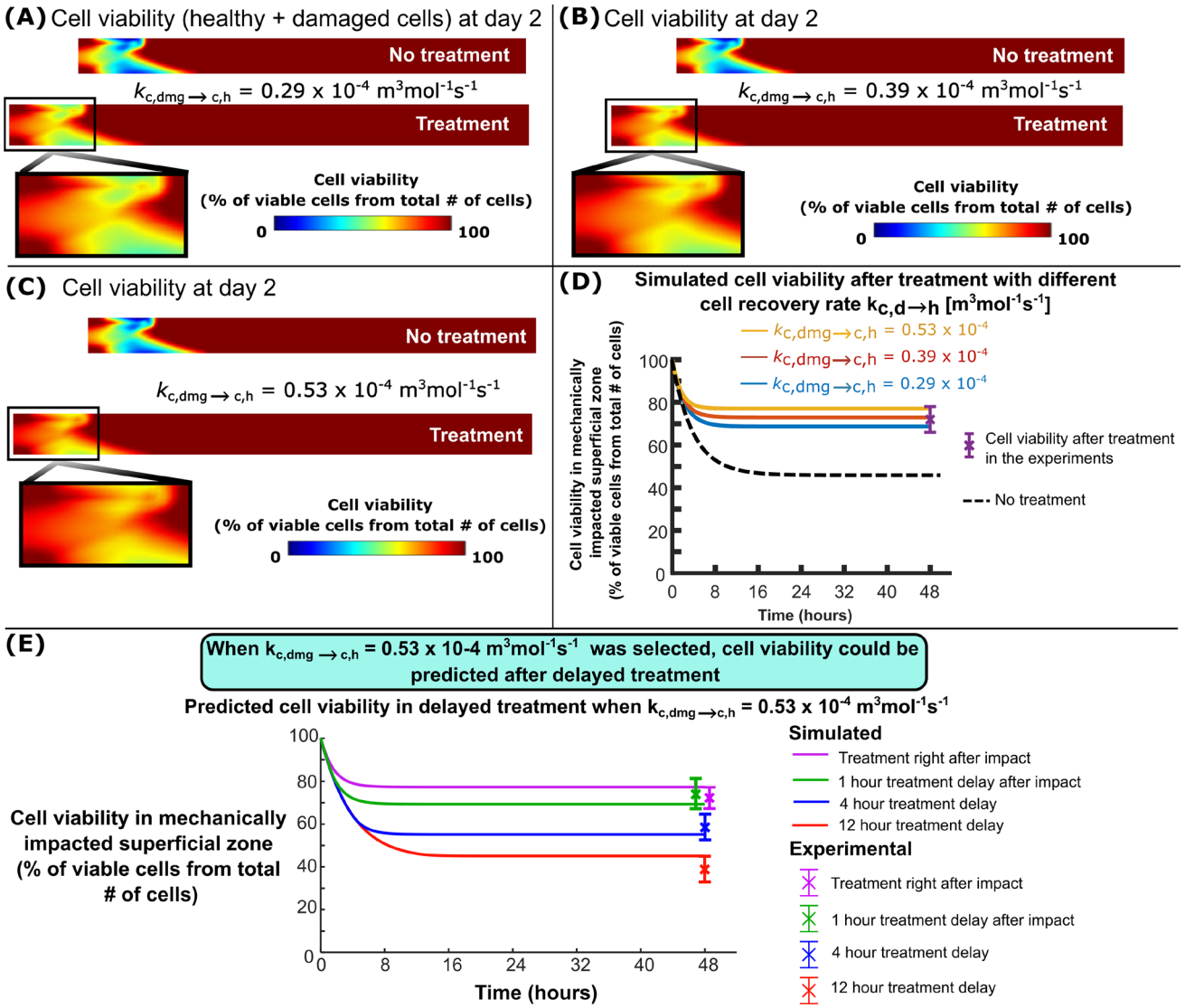

Fig. 5 Cell viability after treatment. Cell viability distributions 2 days after impact when **A** chondrocyte protection rate $k_{c,dmg \rightarrow c,h} = 2.9 \cdot 10^{-5}$ m^{3}mol^{-1} s^{-1}, **B** when $k_{c,dmg \rightarrow c,h} = 3.9 \cdot 10^{-5}$ m^{3}mol^{-1} s^{-1} and when C) $k_{c,dmg \rightarrow c,h} = 5.3 \cdot 10^{-5}$ m^{3}mol^{-1} s^{-1}. **D** Simulated and experimentally measured cell viability in the superficial zone of the impacted area over 2 days. **E** Comparison of the simulated and experimentally measured cell viability after 0-, 1-, 4-, and 12-h treatment delay. With reference parameter $k_{c,dmg \rightarrow c,h} = 5.3 \cdot 10^{-5}$ m^{3}mol^{-1} s^{-1}, our model was able to replicate the cell viability after treatment delay as observed in experiments

(Martin et al. 2009). The reference model also showed the best fit to the experimentally observed cell viability over the entire 3 days after impact, showing 64% cell viability 4 h after impact (Fig. 4E). In contrast, with $k_{c,dmg \rightarrow c,dead} = 13.9 \cdot 10^{-5}$ s^{-1} and $k_{c,dmg \rightarrow c,dead} = 4.6 \cdot 10^{-5}$ s^{-1}, the model overestimated (viability 51% at 4 h) and underestimated (viability 72% at 4 h) the average cell death, respectively, compared to experiments during the first hours post-impact.

In the case of immediate NAC treatment post-impact, increasing the chondrocyte protection rate ($k_{c,dmg \rightarrow c,h}$) resulted in further improvements in predicted cell viability two days post-impact, especially at the superficial cartilage (Fig. 5A–C). With 2 day NAC treatment and $k_{c,dmg \rightarrow c,h} = 0.29 \cdot 10^{-4}$ m^{3}mol^{-1} s^{-1} in the model, the predicted cell viability was increased from 46% (no NAC treatment) to 69% in the impacted superficial zone (Fig. 5D), while with $k_{c,dmg \rightarrow c,h} = 0.39 \cdot 10^{-4}$ m^{3}mol^{-1} s^{-1} or $k_{c,dmg \rightarrow c,h} = 0.53 \cdot 10^{-4}$ m^{3}mol^{-1} s^{-1}, the predicted cell viabilities due to treatment were increased to 73 and 77%, respectively. When $k_{c,dmg \rightarrow h} = 0.29 \cdot 10^{-4}$ m^{3}mol^{-1} s^{-1} and $k_{c,dmg \rightarrow h} = 0.39 \cdot 10^{-4}$ m^{3}mol^{-1} s^{-1} was used, the model underestimated cell viability when the treatment was delayed compared to the experiments (data not shown). When $k_{c,dmg \rightarrow h} = 0.53 \cdot 10^{-4}$ m^{3}mol^{-1} s^{-1} was used in the model,

cell viabilities were reduced from 77 to 45% as a function of the NAC treatment delay from 0 to 12 h, respectively (Fig. 5E).

4 Discussion

We developed a computational modeling framework to simulate impact-induced early-phase cell damage (oxidative stress), cell death, proteoglycan degeneration, and short-term anti-oxidative NAC treatment aiming to counteract the biological effects of the impact. We calibrated the model against quantitative data of cell viability and proteoglycan loss from previous *ex vivo* experiments (Martin et al. 2009). The main findings were: i) high shear strains in the impacted region of cartilage can lead to cellular damage and oxidative stress, triggering cell death and proteoglycan degeneration, ii) inhibition of impact-induced oxidative cell damage and cell death with NAC resulted in reduced proteolytic enzyme activity and production (Eq. 15), thereby mitigating proteoglycan loss and iii) since ongoing proteolytic enzyme production was not inhibited, delayed (> 4 h) treatment may not protect the proteoglycan content despite the fact that cell death could be reduced by NAC.

4.1 Simulated cell damage and cell viability after impact

Cell damage was observed in the superficial and deep cartilage due to high shear strains (Brouillette et al. 2014; Bartell et al. 2015, 2020) leading to accumulated cell death over 2 days after impact (Fig. 3). This is also consistent with earlier cartilage impact loading experiments that have reported post-impact cell death in superficial and deep cartilage layers (Goodwin et al. 2010; Rosenzweig et al. 2012; Stolberg-Stolberg et al. 2013; Bartell et al. 2020). Furthermore, our simulations predicted 56% cell damage immediately after impact, in line with the earlier *ex vivo* reports showing harmful ROS production in 60% of superficial chondrocytes 1 h after impact (Goodwin et al. 2010) and 55% viability (Fig. 4D) after 3 days (Martin et al. 2009). Similarly, other *ex vivo* impact models have shown that there is a connection between lethal oxidative stress, oxidative stress associated cell damage, and subsequent cell death within an hour after impact (Bartell et al. 2020). Acute cell death within hours after impact can include different types of cell death such as necrosis and subacute apoptosis (Chen et al. 2001), both promoted by excessive amounts of ROS (Charlier et al. 2016). In the current model, net cell death rate considering both necrosis and apoptosis was used to replicate rapid cell death (Martin et al. 2009) and different cell death types were not considered. However, a large number of necrotic cells could influence net cell death rate in early time-points post-impact and limit the timeframe when NAC can inhibit oxidative stress in lethally damaged cells. Nevertheless, inclusion of necrosis and apoptosis separately has been done in earlier computational models (Kosonen et al. 2023), and it could be included in the current modeling workflow when more experimental data become available.

Our simulations showed that immediately administered NAC treatment reduced acute cell death during the first hours after impact by inhibiting cellular oxidative damage (Fig. 3A). With a high chondrocyte protection rate ($k_{c,dmg\rightarrow c,h} = 5.3 \bullet 10^{-5} m^3 mol^{-1} s^{-1}$), simulated cell viability increased from 46 to 77% in 2 days after impact compared to untreated cartilage in agreement with a 32%-point increase seen in the *ex vivo* experiments (Martin et al. 2009) (Fig. 5D). Similar efficiency of NAC was reported in human *ex vivo* experiments: 14%-point increase in cell viability after 1-day NAC treatment (2 mM) (Riegger et al. 2016) and an increase of over 20%-points after 7-day continuous (medium changed every 2–3 days) treatment of impacted cartilage compared to untreated samples (Riegger et al. 2018). Simulation results suggest that NAC could inhibit loss of cell viability throughout the tissue by counteracting cellular oxidative damage in superficial and deep zones of injured cartilage because of fast diffusion of NAC (small molecular size) to damaged regions.

After 1-, 4- and 12-h post-impact treatment delays, our model predicted 69%, 55%, and 45% cell viability compared to 74 ± 7%, 59 ± 6%, and 39 ± 6% cell viability, respectively, in the previous experiments (Martin et al. 2009) after a single administration of NAC (Fig. 5E). An earlier *ex vivo* human study reported that 7 days of continuous NAC treatment after a 24-h delay could effectively increase cell viability above that of untreated samples after impact (0.59 J) (Riegger et al. 2016). This result could imply that with low impact energies, delayed administration of NAC after impact may still remain effective than currently suggested by our modeling framework (4 h). Although not simulated here, also estimating different impact energies and the associated different cell death rates affected by pro-inflammatory cytokines (Kosonen et al. 2023) is possible in the current modeling framework.

4.2 Proteoglycan content after impact

Without treatment, impact loading can trigger oxidative stress-related proteoglycan degeneration in cartilage (Riegger et al. 2016; Coleman et al. 2018). Our model showed 85% relative proteoglycan content at day 14 which was consistent with 88 ± 10% relative proteoglycan content measured in the experiments (Martin et al. 2009) (Fig. 3C). The lowest proteoglycan content was observed in the superficial zone, which has been also reported in previous *ex vivo*

studies of injuriously loaded cartilage (Eskelinen et al. 2022) which could be driven by mechanical disruption of cartilage, loss of biosynthesis and increased proteolytic activity (Riegger et al. 2016; Eskelinen et al. 2022). In our earlier model (Kosonen et al. 2023), we showed that over short periods, proteolytic enzyme production is more important to induce loss of proteoglycan content than cell death and impaired biosynthesis in injured and physiologically, cyclically loaded cartilage. This same mechanism is present in the current study which suggests that decrease of proteoglycan biosynthesis was not the primary mechanism for the proteoglycan loss after impact. Hence, acute ROS inhibition by NAC could be important to effectively inhibit proteoglycan loss caused by catabolic cell reactions.

When NAC treatment was utilized immediately after impact (time 0) and after 4-h delay, our simulations indicated that relative proteoglycan content in the impacted region (compared to the intact area) was increased by 10%-points and 3%-points compared to untreated cartilage at day 14, respectively (Fig. 3C). On average, the experiments reported an average increase of 22%-points in relative proteoglycan content on day 14 when treatment was not delayed (Martin et al. 2009). Our modeling results suggest that after a 4-h delay, treatment is no longer effective in reducing proteoglycan loss although it is still able to reduce cell death. Thus, our model suggests that acute inhibition of impact- and oxidative stress-related stimulation of catabolic enzymes (such as a disintegrin and metalloproteinase with thrombospondin-like motifs (ADAMTS)-4 and -5 (Stanton et al. 2005; Glasson et al. 2007; Zhang et al. 2013)) may play an important role in preventing proteoglycan loss with NAC treatment (Riegger et al. 2016; Riegger and Brenner 2020). However, in addition to reduced oxidative stress and cell damage, other mechanisms may also affect NAC-induced reduction in proteoglycan loss (Fig. 3C), such as an increase of proteoglycan biosynthesis by increased anabolic activities in cells (Riegger et al. 2016; Heywood and Lee 2017), reduction of direct ROS-induced proteoglycan oxidation (Hines et al. 2022), and inhibited inflammatory response of chondrocytes (Homandberg et al. 1997; Setti et al. 2021). However, further research is needed to decipher the effect of each of these variables.

4.3 Limitations

Even though our computational modeling framework was able to replicate the experimentally observed cell viability and proteoglycan content, there are some limitations regarding its biomechanical and biochemical aspects. Our biomechanical simulations of the impact and the resulting strain distributions are dependent on the estimated material properties, cartilage thickness, and depth-dependent structural properties. Also, the maximum shear strain threshold defining the initiation of cell damage (40%) (Orozco et al. 2018) and maximum cell damage (150%) (Argote et al. 2019) were based on earlier computational studies reporting cell death in areas exceeding the tissue-level strain-thresholds, but experiments have shown smaller cell-level strains causing cell death and damage (Bonnevie et al. 2018). These uncertainties may affect simulated strain distribution and initial cell damage distribution in cartilage, which may also influence the spatial NAC treatment effects predicted by our model. However, earlier studies have quantified cell deformation in near real time during dynamic (Komeili et al. 2021) and static (Han et al. 2018) loading, and similar techniques combined with cell viability analysis may enable quantification of high strain-induced cell death after impact.

Besides ECM deformation, chondrocyte responses to the mechanical microenvironment during impact loading may also be influenced by other mechanical factors, such as fluid flow or pressure (Fig. S3 in the supplementary material section S2), which can alter the expression of catabolic enzymes and proteoglycan biosynthesis (Hall et al. 1991; Wang et al. 2020). In the current model, most of the impact load was carried by the collagen network and pressurized interstitial fluid, with less effect from the non-fibrillar matrix. We modeled fluid pressurization during high loading rate impact with a continuum cartilage material via Darcy's law and deformation-dependent permeability. In our model, fluid pressurization influenced deformation of cartilage and subsequent chondrocyte damage, release of proteolytic enzymes and proteoglycan biosynthesis. Chondrocyte damage and downstream cell reactions due to excessive fluid pressure could be also modeled by decreasing the amount of healthy cells with a similar damage function as presented in Eq. (11) (Eskelinen et al. 2024).

We included biochemical tissue degeneration and adaptation mechanisms that have the most experimental and computational support from literature. However, the resulting model remained simplified from *ex vitro*/*in vivo* conditions. The excluded mechanisms were inflammatory response of injured cartilage (Lieberthal et al. 2015), release of damage-associated molecular patterns (Rosenberg et al. 2017), degeneration caused by chondrocyte differentiation (Rim et al. 2020), altered NAC transport due to molecular charge of NAC (Kar et al. 2016b) and decrease in NAC concentration via chemical reactions and uptake in the cells (Zafarullah et al. 2003; Pedre et al. 2021). Since decrease in NAC concentration over time was not considered, our model may underestimate the efficiency of NAC because it would be smaller concentration of NAC that actually causes the protection found against cell damage. In addition, our current model does not consider surface roughness, cartilage lesions or damage of osteochondral junction resulting from the impact loading, all of which could affect diffusion, convective transport of different biomolecules and fluid leakage

out from the cartilage. This fluid leakage could also lead to lower interstitial fluid pressure, resulting in higher strains than those currently estimated by the model, thus, affecting cell damage and proteoglycan loss post-impact (Liao et al. 2019, 2020; Li et al. 2023). Yet, our model offers a novel way to study temporal effects of degeneration and antioxidative treatments *ex vivo*, and augmenting the mechanisms in this baseline model would be the next step toward simulating cartilage degeneration and treatment-induced regeneration *in vivo*. Nevertheless, extensive experimental calibration and more quantitative data (for example, gene expression, immunohistochemical analysis, and experiments with/without proteolytic enzyme-inhibitors to analyze NAC effects spatially and temporally) are needed to augment the current model with new mechanisms.

4.4 Future directions

In the future, this new modeling framework can be augmented with our previous modeling framework to simulate time-dependent cyclic loading and inflammation post-impact (Kosonen et al. 2023). When cyclic loading post-impact is included in the modeling framework, it could be used to simulate the molecular advection/diffusion of cytokines/growth factors within deformed cartilage and the cell responses to interstitial fluid flow. Moreover, the model could be enhanced to consider the effect of cartilage degeneration on the material properties (Zhang et al. 2009; Eskelinen et al. 2024). These enhancements would enable simulations of time-dependent effects of treatment administration, sustained drug delivery, and multiple drug treatments to mitigate cartilage degeneration (Zhao et al. 2023). Moreover, to advance this new modeling framework, the following biomechanical and biological data are needed: sample-specific material properties, fraction of damaged cells experiencing oxidative stress, location-specific reduction of damaged cells by NAC, fraction of live and dead cells, and quantitative data on proteoglycan content at several time-points post-impact. In addition, to analyze NAC uptake into cartilage and treatment effects in physiologically loaded cartilage, more data will be needed about possible lesions after impact, tissue structure and content, and activity of proteolytic enzymes within the cartilage. To gather these data, we will conduct new *ex vivo* experiments. Combining the calibrated cell–tissue-level model into state-of-the-art joint-level degeneration models with patient-specific joint geometries, contact forces and inflammation (Orozco et al. 2022; Esrafilian et al. 2024), the model could then be used to guide the most optimal treatment strategies to mitigate PTOA progression.

5 Conclusions

We developed a novel computational modeling framework to study NAC treatment mechanisms on mitigating cartilage degeneration through overloading-driven cell damage. Our simulations were comparable to previous experiments showing reduced impact-related cell damage, proteolytic activity, and proteoglycan loss after NAC treatment. The developed modeling framework enhances understanding of the role of cell damage and oxidative stress on cartilage degeneration and time-dependent NAC treatment mechanisms post injurious loading of cartilage. Although definitive treatment has yet to be discovered for PTOA, our new modeling framework could aid the development of better treatment strategies. In the future, our modeling framework could help optimizing NAC dosage and timing for cartilage treatment to better inhibit cell death and cartilage degeneration after injurious loading.

Supplementary Information The online version contains supplementary material available at https://doi.org/10.1007/s10237-025-01961-8.

Acknowledgements We acknowledge the support of University of Eastern Finland, Massachusetts Institute of Technology and University of Iowa to conduct this research.

Author contributions Kosonen JP contributed to conceptualization, data curation, formal analysis, investigation, methodology, software, validation, visualization, writing—original draft preparation. Eskelinen ASA contributed to conceptualization, data curation, investigation, methodology, software, validation, writing—review & editing. Orozco GA contributed to conceptualization, data curation, investigation, methodology, software, writing—review & editing. Coleman MC, Anderson DD, and Goetz JE contributed to conceptualization, methodology, supervision, writing—review & editing. Grodzinsky AJ contributed to conceptualization, methodology, supervision, writing—review & editing. Tanska P and Korhonen RK contributed to conceptualization, funding acquisition, investigation, methodology, project administration, resources, supervision, writing—review & editing.

Funding Open access funding provided by University of Eastern Finland (including Kuopio University Hospital). We acknowledge funding support from the Doctoral Programme in Science, Forestry and Technology (LUMETO), Emil Aaltonen Foundation, Novo Nordisk Foundation (grant no. NNF21OC0065373, the Center for Mathematical Modeling of Knee Osteoarthritis (MathKOA)), strategic funding of the University of Eastern Finland, Research Council of Finland (#354916, #363459), Päivikki and Sakari Sohlberg Foundation (#240074), Maire Lisko Foundation, Sigrid Juselius Foundation (#240098).

Data availability All the underlying data will be made available in IDA Research Data Storage Service (https://etsin.fairdata.fi/dataset/253f16b6-5b7e-4293-abad-6561ee7ee0d3157; https://doi.org/10.23729/fd-8a9a1a33-6221-3b64-a583-5df1d5d81e4e). Accession numbers will be available after acceptance of the manuscript for publication.

Declarations

Conflict of interest The authors declare no competing interests.

References

Aldini G, Altomare A, Baron G et al (2018) N-Acetylcysteine as an antioxidant and disulphide breaking agent: the reasons why. Free Radic Res 52:751–762. https://doi.org/10.1080/10715762.2018.1468564

Anderson DD, Chubinskaya S, Guilak F et al (2011) Post-traumatic osteoarthritis: improved understanding and opportunities for early intervention. J Orthop Res 29:802–809. https://doi.org/10.1002/jor.21359

Argote PF, Kaplan JT, Poon A et al (2019) Chondrocyte viability is lost during high-rate impact loading by transfer of amplified strain, but not stress, to pericellular and cellular regions. Osteoarthritis Cartilage 27:1822–1830. https://doi.org/10.1016/j.joca.2019.07.018

Bartell LR, Fortier LA, Bonassar LJ, Cohen I (2015) Measuring microscale strain fields in articular cartilage during rapid impact reveals thresholds for chondrocyte death and a protective role for the superficial layer. J Biomech 48:3440–3446. https://doi.org/10.1016/j.jbiomech.2015.05.035

Bartell LR, Fortier LA, Bonassar LJ et al (2020) Mitoprotective therapy prevents rapid, strain-dependent mitochondrial dysfunction after articular cartilage injury. J Orthop Res 38:1257–1267. https://doi.org/10.1002/jor.24567

Bonnevie ED, Delco ML, Bartell LR et al (2018) Microscale frictional strains determine chondrocyte fate in loaded cartilage. J Biomech 74:72–78. https://doi.org/10.1016/j.jbiomech.2018.04.020

Brouillette MJ, Ramakrishnan PS, Wagner VM et al (2014) Strain-dependent oxidant release in articular cartilage originates from mitochondria. Biomech Model Mechanobiol 13:565–572. https://doi.org/10.1007/s10237-013-0518-8

Burgin LV, Aspden RM (2007) A drop tower for controlled impact testing of biological tissues. Med Eng Phys 29:525–530. https://doi.org/10.1016/j.medengphy.2006.06.002

Charlier E, Relic B, Deroyer C et al (2016) Insights on molecular mechanisms of chondrocytes death in osteoarthritis. Int J Mol Sci. https://doi.org/10.3390/ijms17122146

Chen CT, Burton-Wurster N, Borden C et al (2001) Chondrocyte necrosis and apoptosis in impact damaged articular cartilage. J Orthop Res 19:703–711. https://doi.org/10.1016/S0736-0266(00)00066-8

Coleman MC, Ramakrishnan PS, Brouillette MJ, Martin JA (2016) Injurious loading of articular cartilage compromises chondrocyte respiratory function. Arthritis Rheumatol 68:662–671. https://doi.org/10.1002/art.39460

Coleman MC, Brouillette MJ, Andresen NS et al (2017) Differential effects of superoxide dismutase mimetics after mechanical overload of articular cartilage. Antioxidants 6:1–10. https://doi.org/10.3390/antiox6040098

Coleman MC, Goetz JE, Brouillette MJ et al (2018) Targeting mitochondrial responses to intra-articular fracture to prevent posttraumatic osteoarthritis. Sci Transl Med 10:5372

Didomenico CD, Lintz M, Bonassar LJ (2018) Molecular transport in articular cartilage - what have we learned from the past 50 years? Nat Rev Rheumatol 14:393–403. https://doi.org/10.1038/s41584-018-0033-5

Ding L, Guo D, Homandberg GA et al (2014) A single blunt impact on cartilage promotes fibronectin fragmentation and upregulates cartilage degrading stromelysin-1/matrix metalloproteinase-3 in a bovine ex vivo model. J Orthop Res 32:811–818. https://doi.org/10.1002/jor.22610

Elahi SA, Castro-Viñuelas R, Tanska P et al (2023) Contribution of collagen degradation and proteoglycan depletion to cartilage degeneration in primary and secondary osteoarthritis: an in silico study. Osteoarthritis Cartilage 31:741–752. https://doi.org/10.1016/j.joca.2023.01.004

Eskelinen ASA, Mononen ME, Venäläinen MS et al (2019) Maximum shear strain-based algorithm can predict proteoglycan loss in damaged articular cartilage. Biomech Model Mechanobiol 18:753–778. https://doi.org/10.1007/s10237-018-01113-1

Eskelinen ASA, Tanska P, Florea C et al (2020) Mechanobiological model for simulation of injured cartilage degradation via pro-inflammatory cytokines and mechanical. PLoS Comput Biol 16:1–25. https://doi.org/10.1371/journal.pcbi.1007998

Eskelinen ASA, Florea C, Tanska P et al (2022) Cyclic loading regime considered beneficial does not protect injured and interleukin-1-inflamed cartilage from post-traumatic osteoarthritis. J Biomech. https://doi.org/10.1016/j.jbiomech.2022.111181

Eskelinen ASA, Kosonen JP, Hamada M, et al (2024) Time-dependent computational model of post-traumatic osteoarthritis to estimate how mechanoinflammatory mechanisms impact cartilage aggrecan content. bioRxiv 2024.10.08.617186; https://doi.org/10.1101/2024.10.08.617186

Esrafilian A, Halonen KS, Dzialo CM et al (2024) Effects of gait modifications on tissue-level knee mechanics in individuals with medial tibiofemoral osteoarthritis: a proof-of-concept study towards personalized interventions. J Orthop Res 42:326–338. https://doi.org/10.1002/jor.25686

Glasson SS, Askew R, Sheppard B et al (2007) Erratum: Deletion of active ADAMTS5 prevents cartilage degradation in a murine model of osteoarthritis (Nature (2005) 434, 644–648)). Nature 446:102. https://doi.org/10.1038/nature05640

Goodwin W, McCabe D, Sauter E et al (2010) Rotenone prevents impact-induced chondrocyte death. J Orthop Res 28:1057–1063. https://doi.org/10.1002/jor.21091

Hall AC, Urban JPG, Gehl KA (1991) The effects of hydrostatic pressure on matrix synthesis in articular cartilage. Journal of Orthopaedic Research 9:1–10. https://doi.org/10.1002/jor.1100090102

Han SK, Ronkainen AP, Saarakkala S et al (2018) Alterations in structural macromolecules and chondrocyte deformations in lapine retropatellar cartilage 9 weeks after anterior cruciate ligament transection. J Orthop Res 36:342–350. https://doi.org/10.1002/jor.23650

Heiner AD, Smith AD, Goetz JE et al (2013) Cartilage-on-cartilage versus metal-on-cartilage impact characteristics and responses. J Orthop Res 31:887–893. https://doi.org/10.1002/jor.22311

Heywood HK, Lee DA (2017) Bioenergetic reprogramming of articular chondrocytes by exposure to exogenous and endogenous reactive oxygen species and its role in the anabolic response to low oxygen. J Tissue Eng Regen Med 11:2286–2294. https://doi.org/10.1002/term.2126

Hines MR, Goetz JE, Gomez-Contreras PC et al (2022) Extracellular biomolecular free radical formation during injury. Free Radic Biol Med 188:175–184. https://doi.org/10.1016/j.freeradbiomed.2022.06.223

Hodgkinson T, Kelly DC, Curtin CM, O'Brien FJ (2022) Mechanosignalling in cartilage: an emerging target for the treatment of

osteoarthritis. Nat Rev Rheumatol 18:67–84. https://doi.org/10.1038/s41584-021-00724-w
Homandberg GA, Wen C, Hui F (1997) Agents that block fibronectin fragment-mediated cartilage damage also promote repair. Inflamm Res 46:467–471. https://doi.org/10.1007/s000110050226
Hosseini SM, Wilson W, Ito K, Van Donkelaar CC (2014) A numerical model to study mechanically induced initiation and progression of damage in articular cartilage. Osteoarthritis Cartilage 22:95–103. https://doi.org/10.1016/j.joca.2013.10.010
Huyghe JM, Houben GB, Drost MR, van Donkelaar CC (2003) An ionised/non-ionised dual porosity model of intervertebral disc tissue. Biomech Model Mechanobiol 2:3–19. https://doi.org/10.1007/s10237-002-0023-y
Jadin KD, Wong BL, Bae WC et al (2005) Depth-varying density and organization of chondrocytes in immature and mature bovine articular cartilage assessed by 3D imaging and analysis. J Histochem Cytochem 53:1109–1119. https://doi.org/10.1369/jhc.4A6511.2005
Jeffrey JE, Aspden RM (2006) The biophysical effects of a single impact load on human and bovine articular cartilage. Proc Inst Mech Eng H 220:677–686. https://doi.org/10.1243/09544119JEIM31
Jeffrey JE, Gregory DW, Aspden RM (1995) Matrix damage and chondrocyte viability following a single impact load on articular cartilage. Arch Biochem Biophys 322:87–96. https://doi.org/10.1006/abbi.1995.1439
Julkunen P, Kiviranta P, Wilson W et al (2007) Characterization of articular cartilage by combining microscopic analysis with a fibril-reinforced finite-element model. J Biomech 40:1862–1870. https://doi.org/10.1016/j.jbiomech.2006.07.026
Kapitanov GI, Wang X, Ayati BP et al (2016) Linking cellular and mechanical processes in articular cartilage lesion formation: a mathematical model. Front Bioeng Biotechnol. https://doi.org/10.3389/fbioe.2016.00080
Kar S, Smith DW, Gardiner BS et al (2016a) Modeling IL-1 induced degradation of articular cartilage. Arch Biochem Biophys 594:37–53. https://doi.org/10.1016/j.abb.2016.02.008
Kar S, Smith DW, Gardiner BS, Grodzinsky AJ (2016b) Systems based study of the therapeutic potential of small charged molecules for the inhibition of IL-1 mediated cartilage degradation. PLoS ONE 11:1–38. https://doi.org/10.1371/journal.pone.0168047
Komeili A, Otoo BS, Abusara Z et al (2021) Chondrocyte deformations under mild dynamic loading conditions. Ann Biomed Eng 49:846–857. https://doi.org/10.1007/s10439-020-02615-9
Kosonen JP, Eskelinen ASA, Orozco GA et al (2023) Injury-related cell death and proteoglycan loss in articular cartilage: numerical model combining necrosis, reactive oxygen species, and inflammatory cytokines. PLoS Comput Biol 19:1–26. https://doi.org/10.1371/journal.pcbi.1010337
Lepetsos P, Papavassiliou AG (2016) ROS/oxidative stress signaling in osteoarthritis. Biochim Biophys Acta Mol Basis Dis 1862:576–591. https://doi.org/10.1016/j.bbadis.2016.01.003
Li Q, Miramini S, Smith DW et al (2023) Osteochondral junction leakage and cartilage joint lubrication. Comput Methods Programs Biomed. https://doi.org/10.1016/j.cmpb.2023.107353
Liao JJ, Smith DW, Miramini S et al (2019) The investigation of fluid flow in cartilage contact gap. J Mech Behav Biomed Mater 95:153–164. https://doi.org/10.1016/j.jmbbm.2019.04.008
Liao JJ, Smith DW, Miramini S et al (2020) A coupled contact model of cartilage lubrication in the mixed-mode regime under static compression. Tribol Int 145:106185. https://doi.org/10.1016/j.triboint.2020.106185
Lieberthal J, Sambamurthy N, Scanzello CR (2015) Inflammation in joint injury and post-traumatic osteoarthritis. Osteoarthritis Cartilage 23:1825–1834. https://doi.org/10.1016/j.joca.2015.08.015
Mahmoudian A, Lohmander LS, Mobasheri A et al (2021) Early-stage symptomatic osteoarthritis of the knee — time for action. Nat Rev Rheumatol 17:621–632. https://doi.org/10.1038/s41584-021-00673-4
Martin JA, McCabe D, Walter M et al (2009) N-acetylcysteine inhibits post-impact chondrocyte death in osteochondral explants. J Bone Joint Surg—Series A 91:1890–1897. https://doi.org/10.2106/JBJS.H.00545
Nakagawa S, Arai Y, Mazda O et al (2010) N-acetylcysteine prevents nitric oxide-induced chondrocyte apoptosis and cartilage degeneration in an experimental model of osteoarthritis. J Orthop Res 28:156–163. https://doi.org/10.1002/jor.20976
Orozco GA, Tanska P, Florea C et al (2018) A novel mechanobiological model can predict how physiologically relevant dynamic loading causes proteoglycan loss in mechanically injured articular cartilage. Sci Rep 8:1–16. https://doi.org/10.1038/s41598-018-33759-3
Orozco GA, Eskelinen ASA, Kosonen JP et al (2022) Shear strain and inflammation-induced fixed charge density loss in the knee joint cartilage following ACL injury and reconstruction: a computational study. J Orthop Res 40(1505):1522. https://doi.org/10.1002/jor.25177
Ozcamdalli M, Misir A, Kizkapan TB et al (2017) Comparison of intra-articular injection of hyaluronic acid and N-acetyl cysteine in the treatment of knee osteoarthritis: a pilot study. Cartilage 8:384–390. https://doi.org/10.1177/1947603516675915
Pedre B, Barayeu U, Ezeriņa D, Dick TP (2021) The mechanism of action of N-acetylcysteine (NAC): the emerging role of H2S and sulfane sulfur species. Pharmacol Ther. https://doi.org/10.1016/j.pharmthera.2021.107916
Rahman MM, Watton PN, Neu CP, Pierce DM (2023) A chemo-mechano-biological modeling framework for cartilage evolving in health, disease, injury, and treatment. Comput Methods Programs Biomed. https://doi.org/10.1016/j.cmpb.2023.107419
Riegger J, Brenner RE (2020) Pathomechanisms of posttraumatic osteoarthritis: chondrocyte behavior and fate in a precarious environment. Int J Mol Sci. https://doi.org/10.3390/ijms21051560
Riegger J, Joos H, Palm HG et al (2016) Antioxidative therapy in an ex vivo human cartilage trauma-model: attenuation of trauma-induced cell loss and ECM-destructive enzymes by N-acetyl cysteine. Osteoarthritis Cartilage 24:2171–2180. https://doi.org/10.1016/j.joca.2016.07.019
Riegger J, Joos H, Palm HG et al (2018) Striking a new path in reducing cartilage breakdown: combination of antioxidative therapy and chondroanabolic stimulation after blunt cartilage trauma. J Cell Mol Med 22:77–88. https://doi.org/10.1111/jcmm.13295
Riegger J, Leucht F, Palm HG et al (2019) Initial harm reduction by N-acetylcysteine alleviates cartilage degeneration after blunt single-impact cartilage trauma in vivo. Int J Mol Sci. https://doi.org/10.3390/ijms20122916
Riegger J, Schoppa A, Ruths L et al (2023) Oxidative stress as a key modulator of cell fate decision in osteoarthritis and osteoporosis: a narrative review. Cell Mol Biol Lett 28:76
Rim YA, Nam Y, Ju JH (2020) The role of chondrocyte hypertrophy and senescence in osteoarthritis initiation and progression. Int J Mol Sci. https://doi.org/10.3390/ijms21072358
Rosenberg JH, Rai V, Dilisio MF, Agrawal DK (2017) Damage-associated molecular patterns in the pathogenesis of osteoarthritis: potentially novel therapeutic targets. Mol Cell Biochem 434:171–179. https://doi.org/10.1007/s11010-017-3047-4
Rosenzweig DH, Djap MJ, Ou SJ, Quinn TM (2012) Mechanical injury of bovine cartilage explants induces depth-dependent, transient changes in MAP kinase activity associated with apoptosis. Osteoarthritis Cartilage 20:1591–1602. https://doi.org/10.1016/j.joca.2012.08.012
Sauter E, Buckwalter JA, McKinley TO, Martin JA (2012) Cytoskeletal dissolution blocks oxidant release and cell death in injured

cartilage. J Orthop Res 30:593–598. https://doi.org/10.1002/jor.21552
Setti T, Arab MGL, Santos GS et al (2021) The protective role of glutathione in osteoarthritis. J Clin Orthop Trauma 15:145–151. https://doi.org/10.1016/j.jcot.2020.09.006
Siefen T, Bjerregaard S, Borglin C, Lamprecht A (2022) Assessment of joint pharmacokinetics and consequences for the intraarticular delivery of biologics. J Control Release 348:745–759. https://doi.org/10.1016/j.jconrel.2022.06.015
Stanton H, Rogerson FM, East CJ et al (2005) ADAMTS5 is the major aggrecanase in mouse cartilage in vivo and in vitro. Nature 434:648–652. https://doi.org/10.1038/nature03417
Stolberg-Stolberg JA, Furman BD, William Garrigues N et al (2013) Effects of cartilage impact with and without fracture on chondrocyte viability and the release of inflammatory markers. J Orthop Res 31:1283–1292. https://doi.org/10.1002/jor.22348
Torzilli PA, Grigiene R, Borrelli J, Helfet DL (1999) Effect of impact load on articular cartilage: cell metabolism and viability, and matrix water content. J Biomech Eng 121:433–441. https://doi.org/10.1115/1.2835070
Tudorachi NB, Totu EE, Fifere A et al (2021) The implication of reactive oxygen species and antioxidants in knee osteoarthritis. Antioxidants 10:1–29. https://doi.org/10.3390/antiox10060985
Wang LJ, Zeng N, Yan ZP et al (2020) Post-traumatic osteoarthritis following ACL injury. Arthritis Res Ther 22:1–8. https://doi.org/10.1186/s13075-020-02156-5
Wilson W, Van Donkelaar CC, Van Rietbergen B et al (2004) Stresses in the local collagen network of articular cartilage: a poroviscoelastic fibril-reinforced finite element study. J Biomech 37:357–366. https://doi.org/10.1016/S0021-9290(03)00267-7
Wilson W, Van Donkelaar CC, Huyghe JM (2005a) A comparison between mechano-electrochemical and biphasic swelling theories for soft hydrated tissues. J Biomech Eng 127:158–165. https://doi.org/10.1115/1.1835361
Wilson W, Van Donkelaar CC, Van Rietbergen B, et al (2005b) Erratum: A fibril-reinforced poroviscoelastic swelling model for articular cartilage (Journal of Biomechanics (2005) 38 (1195-1204) PII: S0021929004003367 and https://doi.org/10.1016/S0021-9290(03)00267-7). J Biomech 38:2138–2140. https://doi.org/10.1016/j.jbiomech.2005.04.024
Wilson W, Van Donkelaar CC, Van Rietbergen B, Huiskes R (2005c) A fibril-reinforced poroviscoelastic swelling model for articular cartilage. J Biomech 38:1195–1204. https://doi.org/10.1016/j.jbiomech.2004.07.003
Yeh YT, Liang CC, Chang CL et al (2020) Increased risk of knee osteoarthritis in patients using oral N-acetylcysteine: a nationwide cohort study. BMC Musculoskelet Disord 21:1–8. https://doi.org/10.1186/s12891-020-03562-1
Zafarullah M, Li WQ, Sylvester J, Ahmad M (2003) Molecular mechanisms of N-acetylcysteine actions. Cell Mol Life Sci 60:6–20. https://doi.org/10.1007/s000180300001
Zhang L, Bruce GS et al (2009) Integrated model of IGF-I mediated biosynthesis in a deformed articular cartilage. J Eng Mech 135:439–449. https://doi.org/10.1061/ASCE0733-93992009135:5439
Zhang E, Yan X, Zhang M et al (2013) Aggrecanases in the human synovial fluid at different stages of osteoarthritis. Clin Rheumatol 32:797–803. https://doi.org/10.1007/s10067-013-2171-0
Zhao T, Li X, Li H et al (2023) Advancing drug delivery to articular cartilage: from single to multiple strategies. Acta Pharm Sin B 13:4127